

Università degli studi di Trieste

facoltà di scienze matematiche, fisiche e naturali

Corso di Laurea in Fisica

Study of non-perturbative versus tunneling regimes for high harmonic generation in noble gases by ultrashort coherent light pulses

Tesi di Laurea in Fisica Teorica

Relatore:
Chiar.mo Prof.
Fuvio Parmigiani

Presentata da:
Antonio Caretta

Sessione
Anno Accademico 2007/08



Università degli studi di Trieste

FACOLTÀ DI SCIENZE MATEMATICHE, FISICHE E NATURALI

Corso di Laurea in Fisica

Studio di generazione d'armoniche in gas nobile tramite impulsi di luce coerente tra regime non-perturbativo e tunneling

Tesi di Laurea in Fisica Teorica

Relatore:
Chiar.mo Prof.
Fuvio Parmigiani

Presentata da:
Antonio Caretta

Sessione
Anno Accademico 2007/08

Contents

1 Introduction **i**

2 HHG processes **1**

2.1 Strong optical field (pulsed laser) *vs.* bound electrons 2

2.2 Classical model 5

2.2.1 Keldysh theory 6

2.3 The semi-classical picture 10

2.3.1 Fenomenological approach: quantum path 17

2.3.2 Propagation effects 20

2.4 Different ionization processes 22

3 Experimental set-up **27**

3.1 Laser system 27

3.2 Experimental chambers 28

3.3 HHG facility 29

3.3.1 Two-color optical set-up 30

3.3.2 Intensity variation optical set-up 31

4 Measurements and analysis **35**

4.1 IR and second harmonic HHG 35

4.2 Ionization as a function of γ_K 40

4.3 two and three color generation 41

4.4 Data analysis 41

4.4.1 Two color single HHG 41

4.4.2 γ_K parametrization 41

5 Conclusions **43**

Conclusions **43**

A Lewenstein model **45**

Bibliography **47**

Chapter 1

Introduction

When an electromagnetic field (EM), propagating throught space, encounters matter there is no a simple and unique way to describe what happens. One possible way to describe the process is to consider a low energy (and so low amplitude) EM field and use a simple linear function of the amplitude: it is possible, with this approximation, to reduce equations, thanks to power expansion series, to the first perturbative order.
The process, as described above, has obviously a limit: increasing the amplitude of the field, the linear description becomes inaccurate or even wrong and therefore higher order corrections are needed. This improvement introduces the beginning of the so called non-linear analysis.
At this point the phenomenon is harder to describe but, at the same time, the requirements are clear: keeping adding perturbation terms until the physics of the interaction is properly reproduced. This last approach identifies what is called the "perturbative regime". However, taking such process to extreme levels, further results can be observed. By (i) further increasing the amplitude of the EM or (ii) reducing its temporal evolution even the non-linear analysis described above can be whereby influenced. At this stage, the "trick" of adding terms stops giving results and turns impossible to reproduce with the perturbative method what happens: this different behaviour shows the presence of a new regime.

What does cause this dual outcome? When the external field has the same intensity order of the binding atomic potential (Coulomb potential) of matter, the perturbation expansion loses the hypothesis on which it is based: higher fields powers are not anymore negligible and it is clear that the external field isn't anymore a "perturbation". The intensity level at which this occurs strongly depends on the temporal evolution of the incident radiation – the shorter the pulse is the higher this process appears –; but the energy density order needed to reach this regime – called "non-perturbative" or "strong-field" – is about $10^{13}\ W/cm^2$.

This information shows – and moves the interest to – the importance of the field source for these phenomena. After the discovery of the LASER source in 1960 - first predicted by Einstein in 1917 ("Stimulated emission") - in the past fifty years an incredible development was made in the scientific world. Thanks to the property of this type of light new physics were studied and new discovery were made, some of great importance for radiation-matter interaction: the rise time of intense radiation determines the maximum field strength atoms can be exposed to. Lasers generating ultrashort coherent light pulses permit to achieve the energy required to reach the non-perturbative response of atoms. Light wave packets are generated comprising only few oscillations cycles of the electronic and magnetic fields. Reducing the spatial extension of such pulses and focusing them the radiation can be extremely – temporally and spatially – confined to a few cubic micrometers. As a result of this technique it is possible to reach peak intensities higher than $10^{15}\ W/cm^2$ and therefore the amplitude of the electric filed approaches $10^9\ V/cm$. The laser field strength becomes at this stage enough to suppress the binding Coulomb potential in atoms and trigger optical-field ionization (Keldysh 1965).

When the atomic electron is removed far from the nucleus it starts oscillating into the field till it detaches from the binding potential; detachment probability increases with the duration of the radiation. In few-cycle laser fields, high intensities are available which last few optical periods (that means few femtoseconds). Hence detachment of the first electron is completed at higher

field's strengh: optical-ionization rate becomes comparable to the laser oscillating frequency and the electron gains unprecedent kinetic energies (up to and beyond the keV level).

An interesting aspect - deeply analyzed in the past two decades - turns clear at this level: the high energy electron can fall again into its nucleus emitting a single photon. This process is called High-order Harmonic Generation (HHG) because the outgoing photons have only multiple frequencies of the external oscillating field and can be considered "higher harmonics".

Chapter 2

HHG processes

The principal aspect to identify HHG processes is that the foundamental laser frequency is converted to integer multiples during an highly non-linear interaction with matter: many photons are absorbed and then one single photon is emitted. The energy-spectra of the radiation measured after the interaction with the medium, for example a noble gas, has a typical shape that allow to recognize HHG processes: only odd harmonics of the laser frequency are generated and the conversion efficiency does not simply decrease with the increasing of the harmonic order. In fact, there is a region where the intensities of the harmonics are constant.
So, as represented in figure 2.1, three regions can be distinguished:

- perturbative region: the HHG efficiency decreases linearly with the harmonic order;
- plateau region: the efficiency is constant;
- cut-off region: the efficiency decreases again till no harmonic is generated.

In this chapter, in order to create a frame to understand and explain the process, are presented the theoretical models introduced in these years to explain the HHG. The process will be analyzed first with classical mechanics

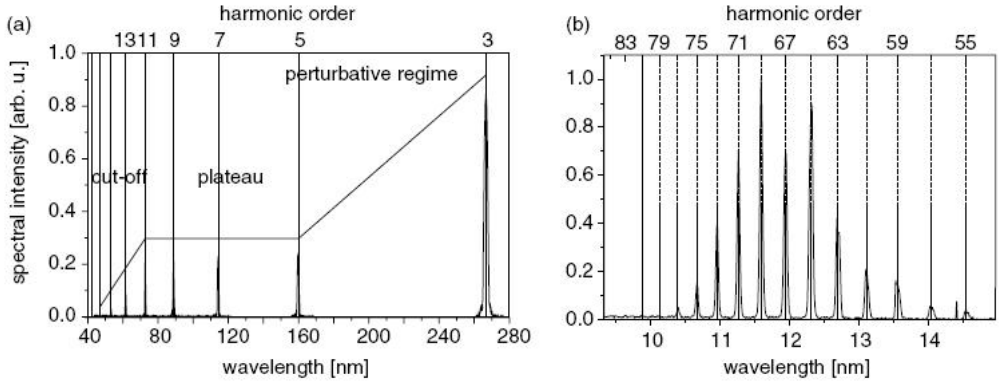


Figure 2.1: (a) Typical HHG spectrum with three specified regions; (b) measured spectrum: lower orders are reduced duo to the presence of a zinconium filter (figure taken from [8]).

in section (2.1), describing in particular the non-linear optical regimes in radiation-matter interaction. Then the propagation of free electrons inside an EM field will be the argument of section (2.2). Two quantum model are presented then in sections (2.3) and (2.4). The first is a semi-classical analysis, and gives a simple and useful picture of the HHG as a three step process: an atomic electron is ionized, it propagates freely inside the EM and it recoils the atom. The last model is the result of a critical analysis of the phenomenon and it represents a general theory for HHG reducing the limitation of the semi-classical model.

2.1 Strong optical field (pulsed laser) *vs.* bound electrons

The nonlinear response of matter, when invested by strong radiation, manifests itself on the equation for the induced polarization P:

$$P = \epsilon_0 \chi^{(1)}\ E + \epsilon_0 \chi^{(2)}\ E^2 + \epsilon_0 \chi^{(3)}\ E^3 + ..., \tag{2.1}$$

where ϵ_0 is the vacuum permeability and $\chi^{(j)}$ is the jth order susceptibility tensor. This formula is a power expansion on the EM field E; the sum of the terms without the linear one is called P_{nl}, non-linear polarization. Such non-linearity originates when the laser field *perturbs* the atomic quantum states (under non-resonant excitation conditions): this regime is called perturative regime.
If the EM is *strong* enough to overwhelm the Coulomb potential, bound electrons can escape before the field inverses its sign; the freed electrons than wiggle and gain kinetic energy until the EM field reserves sign. It is usual to refer to this kind of phenomena as "strong-field" optics or regime (SFR). To define the SFR, it is easier to find the conditions where the perturbative regime description fails.

A first limit can be fixed thanks to a simple mathematical requirement: disregarding bound-free transitions between electronic states, is possible to know whethere the polarization series (2.1) will converge. The required condition is that the ratio

$$\frac{\chi^{(j+1)}E^{j+1}}{\chi^{(j)}E^{j}} \simeq \frac{eEa_B}{\hbar\Delta} = \alpha_{bb} \tag{2.2}$$

is smaller than 1 (where e is the electron charge, a_B the Bohr radius, $\hbar$ Planck's constant and Δ the frequency difference between the ground state and the exited state reached by the electron). This equation comes is the ratio betweem the (j+1)-th term and the previous one: asking to be lower than one is a convergence criterion. Is intresting to observe how such a mathematical request is related to a physical meaning: α_{bb} is the bound-bound transition probability.
On the other hand, in order to analyze electronic bound-free transitions, in 1965 ([10]) Keldysh defined an useful scale parameter, γ_K, as follow:

$$\frac{1}{\gamma_K} = \frac{eE}{\omega_0\sqrt{2mW_b}} = \frac{eEa_B}{\hbar\omega_0} = \alpha_{bf}, \tag{2.3}$$

where m is the electron rest mass, e is its charge, ω_0 is the field frequency and $W_b \ll \omega_0$ is the binding potential of the most weakly bound electron

(i.e. the ionization potential). The request $\alpha_{bf} \ll 1$ prevent bound-free transitions (i.e. ionization): therefore the perturbative regime is defined by $\alpha_{bb}, \alpha_{bf} \ll 1$.
Note that someway the field frequency is always required not to exceed the ionization potential; the quantum meaning of this request is that a single EM photon has not sufficient energy to free the atomic electrons.
To complete the picture of these phenomena it is needed to describe and underline the role of the pulse shape in particular for the strong-field regime. The first condition required is $\gamma_K^{-1} > 1$. Therefore the principal aspect to distinguish the regimes is that the SFR allows bound-free transitions; the laser field is so strong that it suppresses the Coulomb potential and the wave function of most weakly bound electron penetrates and exits the barrier. The result is a "quasistatic" ionization rate following the optical cycles of the field: this process is termed optical-field-ionization.
Before describing the classical mechanism introduced by Corkum [1] a brief comment on the pulse duration τ_p is required. Using longer τ_p the number of ionized atoms, when invested by pulses having a uniform electric field on every cycle, increases. This means that it is possible to complete the ionization even before the SFR is entered. To prevent this multiphoton preionization and to have only strong-field interactions, in the visible/near-infrared spectral range, only few-cycle laser pulses (τ_p in the $10fs$ regime) must be used.

After this introduction on the general properties and characteristics on the perturbative regime and on the strong field regime, the High-order Harmonic Generation process will be analyzed. It is clear that to understand properly these phenomena a quantum mechanical approach is needed. But even such a SFR process, for a while, can be studied with classical mechanics before starting with quantum mechanical methods.

2.2 Classical model

The classical way to study the strong-fields effects is to divide the process into several steps (Kulander '93 [3][4], Corkum ' 93 [2], Paulus '94 [12]): is possible to consider just the classical evolution of the electron trajectories when it reaches the continuum at some time t_0.
The only way to properly analyze the transition from bound to free states is using quantum mechanical approach; but a quantum problem involving an atom, his electrons and a strong EM is impossible to solve exactly even when particular boundary condition are fixed. The typical approach is to distinguish many kinds of ionization in order to reduce the variables of the problem: than every case is separatly studied. Due to the importance of the ionization, the first step of the HHG, it is better to wait for further considerations and focus on them at a later stage (see sections 2.3 and 2.4). It is sufficient to know now that the electron is somehow freed form its nucleus by the strong EM.
The second step to study is the electrons oscillations in the EM field (described with its vector potential $\mathbf{A}(t)$). The electron is considered to be so far from the atomic potential that their interaction can be neglected; so the electron dynamics is described classically. The velocity of an electron in a EM field is

$$m\mathbf{v}(t) = e(\mathbf{A}(t) - \mathbf{A}(t_0)) = \mathbf{p} - e\mathbf{A}(t) \tag{2.4}$$

consisting of a constant part - the drift velocity $v_{drift} = \frac{eA(t_0)}{m}$ related to $E_{drift} = \frac{\mathbf{p}^2}{2m} = \frac{e^2\mathbf{A}(t_0)^2}{2m}$(that can be detected) - and the oscillating term $e\mathbf{A}(t)$. The corresponding energy, using the cycle media $< ... >_T$, is

$$E = \frac{m < \mathbf{v}(t)^2 >_T}{2} = \frac{\mathbf{p}^2}{2m} + \frac{e^2 < \mathbf{A}(t)^2 >_T}{2m} \equiv E_{drift} - U_P \tag{2.5}$$

where $U_P = \frac{e^2 < \mathbf{A}(t)^2 >_T}{2m}$ is the ponderomotive energy. It represents the cycle averaged kinetic energy of the wiggling electron. This is a foundamental parameter for describing the SFR and will be frequently used.
The last step is the electron recoil: it is the "inverse" of the ionization

quantum problem regarding the scattering section between the ion and the high energy electron. As a consequence of the recoiling, a photon is emitted with an odd multiple of the laser frequence. The sequence of these three steps can easily describe the HHG phenomena.
Note that in order to describe the dynamics of the electron the HHG process has been divided into three steps: ionization, free motion inside the laser field and recombination with the ion. This is a "simple man model" first proposed by Corkum [2] and Kulander [3] in '93 and was confirmed by a fully quantum analysis (2.3). So, thanks to few classical considarations, a very useful, for example to evaluate the energy order of the experiment, quantitative parameter was found. Following the temporal order of the physical process every HHG step will be described in the next sections.

2.2.1 Keldysh theory

The first step of the HHG is the ionization. The classical theory is unable to explain what happens to the atom while exposed to the strong EM: a semi-classical quantum theory is needed. The picture of the process is quite simple: an electron is in a quantum energy state inside a Coulomb atomic potential and, at a certain moment, starts to be influenced by a continuous (envelope $f(t) = 1$ and phase $\phi_0 = 0$) electromagnetic wave $\mathbf{E}(t) = \mathbf{E}_0\ cos(\omega t)$:

$$V(\mathbf{r}, t) = -\frac{e^2}{4\pi\epsilon_0 r} + e\mathbf{E}(t) \cdot \mathbf{r}. \tag{2.6}$$

The Coulomb potential can be significantly distorted (figure 2.2), depending on $|\mathbf{E}(t)|$, and the bound electron can tunnel outside: the quantum dynamics is so fast that the EM motion is quasi-static and the problem can be solved as any barrier system. This process is called tunnel ionization and it dates back to 1965, when first predicted by Keldysh ([10]). He calculated the formula for the ionization rate w of an hydrogen atom exposed to a strong field:

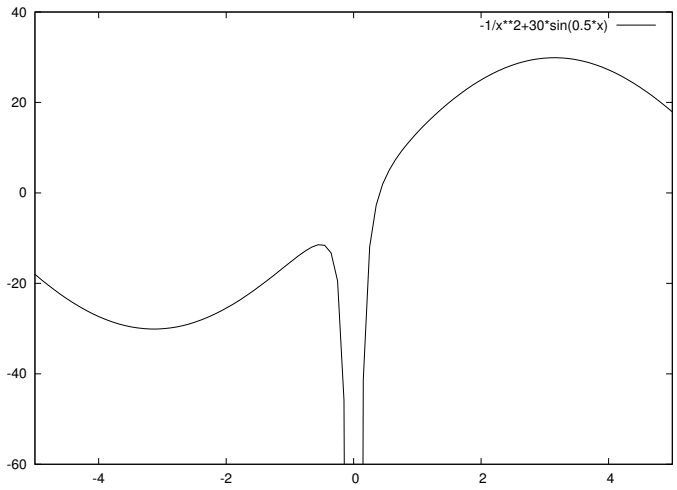


Figure 2.2: The Coulomb potential distorted by a strong EM field.

$$\Gamma_K = \frac{\sqrt{6\pi} I_P}{4\hbar} \left(\frac{eE\hbar}{m^{1/2} I_P^{3/2}} \right)^{1/2} exp \left[-\frac{4\sqrt{2m} I_P^{3/2}}{e\hbar E} \left(1 - \frac{m\omega^2 I_P}{5e^2 E^2} \right) \right] \tag{2.7}$$

(where e is the electron charge and m is its mass, I_P the ionization potential). Note that the rate is related to the free-electron density $n(t)$ by the relation:

$$n(t) = n_0 (1 - e^{-\int_{-\infty}^{t} dt' \Gamma(t')}); \tag{2.8}$$

this equation clearly defines the ionization as a process where the continuum population of electrons increases exponentially until the density is n_0.
Much later in '86 Ammosov, Delone and Krainov generalized Keldysh's theory to arbitrary atoms and initial states ([11]; $C_{ADK}(m,l)$ is a factor depending on the orbital quantum numcers l and m):

$$\Gamma_{ADK} = C_{ADK}(m,l) \sqrt{\frac{E}{(2I_P)^{3/2}}} I_P \left(\frac{2(2I_P)^{3/2}}{E} \right)^{(2/\sqrt{2I_P})-|m|-l} exp \left(-\frac{2(2I_P)^{3/2}}{3E} \right). \tag{2.9}$$

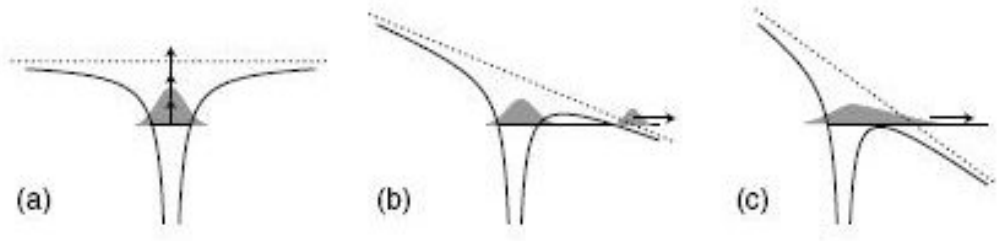


Figure 2.3: Three ionization processes: *a*) multi-photon, *b*) tunneling and *c*) above-threashore ionization [8].

This improvement was of paramount importance in order to explain other different ionization processes: using the same quasi-static picture as before, the deformation of the barrier can be so important that the density electron wave simply overwhelmes it. This is called over-the-barrier, barrier-suppressed ionization or above threashold ionization. Morover an atom can be ionized by many photons with energy lower tha I_P: this process is called Multi Photon Ionization (figure 2.3).

To distinguish these regimes it is helpful to recall another expression of the Keldysh parameter γ_K:

$$\gamma_K = \sqrt{\frac{I_P}{2U_P}}, \tag{2.10}$$

where the pondermotive potential is $U_P = \frac{e^2 E_0^2}{4m\omega^2}$ (the electric field amplitude is $E(t) = E_0 cos(\omega t)$). By the use of this quantity it is possible to determine whether the atom is ionized by tunneling ($\gamma_K \ll 1$) or by multiphoton ionization ($\gamma_K \gg 1$): γ_K parametrizes the ionization process.

The laser-distorted global potential oscillates with the laser frequency. At a low frequency (with respect to the ionization potential), and low γ_K, the distorsion is so "weak" that only tunneling ionization can occour; for higher frequency (and higher γ_K) the quasi-static approximation breaks down and the electron does not have the time to accomodate such fast changes. Its motion is governed by an average field over many laser cycles and no tunneling can succeed because "its time" is shorter than an optical cycle. The stead

nonlinear interaction makes the electron energy increase and finally they are ionized. On the other hand, if the field gets higher and higher it suppresses the barrier and the eletron is then classically "ripped off" the atom: this barrier-suppressed ionization concludes the picture of the first step of the HHG.
Before leaving the classical mechanics approach another important result can be obtained: the HHG cut-off formula. After the electron is ionized, it is accelerated in the EM and it acquires some kinetic energy E_{kin}. If this electron is recoiled by its nucleus it emits a photon with energy equal to

$$\hbar\omega = E_{kin} + I_P. \tag{2.11}$$

The kinetic energy is determined by the ionization time corresponding to a certain phase ϕ of the EM: the Coulomb potential deformation allow ionization every half laser period $T/2$. So the electron recombines before another "rising wave" is coming. The energy gain as a function of the ionization phase ϕ can be plotted numerically solving the equation for the electron position $x(t)$:

$$x(t) = \int_0^t v(t')\,dt' = \frac{E_0 e}{m\omega^2}(cos(\omega t + \phi) - cos(\phi))sin(\phi)t = 0. \tag{2.12}$$

Note that, since the HHG process occurs at every half laser period $T/2$, the dipole momentum, related to $x(t)$, is also expressed with sinusoid functions oscillating at that frequency. Since the Fourier transform of such functions is reduced to a sum on odd terms, this explains why only odd harmonics of the laser frequency are generated.

By observing the shape of the kinetic gain (figure 2.4) some important physical informations can be deduced:

- there is a maximum kinetic energy achievable occuring at $\phi \simeq 18^o$ equal to $\approx 3.17U_P$;
- for each allowed energy gain there are two distinct phases (only at the maximum they are the same).

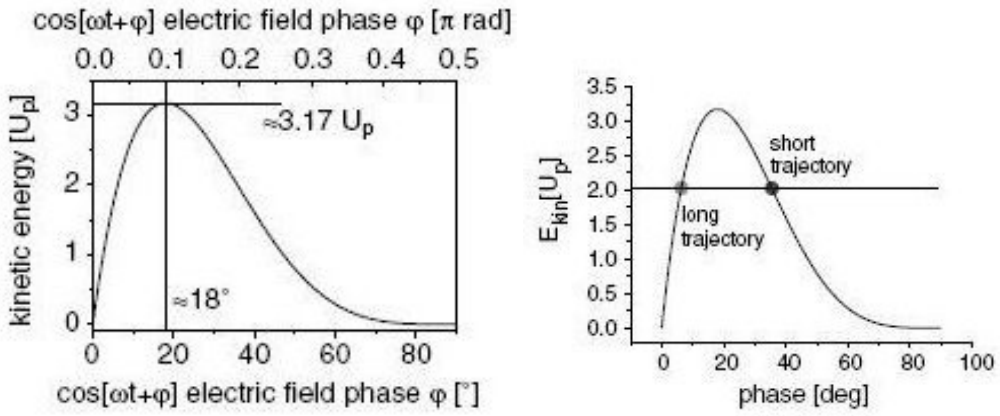


Figure 2.4: Classical energy gain as a function of the ionization phase for an oscillating electron.

So the maximum photon energy, classically calculated, equals to

$$\hbar\omega_{max} \simeq 3.17U_P + I_P. \tag{2.13}$$

Note that in equation 2.13 the equality symbol is not used only because the number 3.17 had been numerically calculated and not because of some approximation made before on the classical model analysis.

2.3 The semi-classical picture

The analysis of HHG can be simplified by using the model of Lewenstein [7] particularly fitting for the tunneling regime. One important result is the derivation of the quantum-mechanical cut-off law.
Consider an atom in Single-Electron Approximation invested by a linearly (in the x direction) polarized laser field $E\ cos(\omega t)$ (atomic units are used and the energies are expressed with respect to the photon energy: $\omega = 1$). The system $|\Psi(t)\rangle$, from the ground state, evolves in time according to the Schroedinger equation

$$i\frac{\partial}{\partial t}|\Psi(t)\rangle = \left[-\frac{\nabla}{2} + V(x) - Ecos(t)x\right]|\Psi(t)\rangle. \tag{2.14}$$

Some typical boundary conditions - for example the fact that $I_P \ll 1$ or that $U_P \leq I_P$ - suggest some basic assumptions:

- no bound state, with except for the ground state $|0\rangle$, contributes to the process;
- the depletion of the ground state, assuming that $U_P < U_{sat}$ (U_{sat} being the saturation level when all atoms ionize during the interaction time), can be neglected - note that with these assumptions the tunneling theory becomes valid - ;
- the intensities are large enough ($10^{14} - 10^{15} W/cm^2$) to treat the electrons in the continuum as free particles not experiencing the potential $V(t)$.

Those limitations hold when there are no intermediate resonances and when the Keldysh parameter $\gamma_K = \sqrt{I_P/2U_P}$ is smaller than 1, i.e. in the tunneling regime.
The wave function must be expanded on the electron quantum states involved in HHG processes: $|0\rangle$, the bound atomic ground state with amplitude $a(t) \simeq 1$ and the continuum states $\{|v\rangle\}_v$ of the propagating electron inside the EM field, with amplitudes $b(v,t)$. So the amplitude distribution on these allowed states can be expressed as:

$$|\Psi(t)\rangle = e^{iI_P t} \left(a(t)|0\rangle + \int b(v,t)|v\rangle \, d^3v \right). \tag{2.15}$$

The amplitude $a(t)$ and $b(v,t)$ completely determine the HHG dynamics throught the evolution of $|\Psi(t)\rangle$:

1. the electron ionization is expressed by the transitions from $|0\rangle$ to $|v\rangle$;
2. the propagation in the EM field is expressed by $|v\rangle$;
3. the electron recoil is related to $|v\rangle$-$|0\rangle$ transitions and to the corresponding emitted photon.

So it is very important to accurately choose the continuum states. Since the electron is considered free from the Coulomb potential is possible to introduce the vector potential $\mathbf{A}(t)$ in the time dependent Schroedinger equation for the electron wave function $\psi(x,t)$ by the minimal coupling:

$$i\hbar\frac{\partial\psi(x,t)}{\partial t} = \frac{1}{2}(-i\hbar\nabla - \mathbf{A}(t))^2\psi(x,t) \tag{2.16}$$

The equation can be solved also for the Fourier transform $\tilde{\psi}(p,t)$ in the p-space:

$$\begin{aligned}\tilde{\psi}(p,t) &= \tilde{\psi}(p,t_0)exp\left(-\frac{i}{\hbar}\int_{t_0}^{t} d\tau\frac{(p-A(t))^2}{2}\right) \\ &\equiv \tilde{\psi}(p,t_0)\ e^{-i/\hbar\ \Phi_V(p,t,t_0)}.\end{aligned} \tag{2.17}$$

This formal solution (and its conjugate on the x-space) is called the Volkov state. Since $\Phi_V(p,t,t_0)$[1], the Volkov phase, completely determines the evolution of this system it is very important for any process, as HHG, involving electrons propagating inside an EM.
So, choosing these continuum states, from the Schroedinger eq. 2.14, neglecting the ground state depletion (i.e. $a(t)=1$), the evolution of $b(v,t)$ can be deduced:

$$\dot{b(v,t)} = -i\left(\frac{v^2}{2} + I_P\right)b(v,t) - E\ cos(t)\frac{\partial b(v,t)}{\partial v_x} + i\ Ecos(t)\ d_x(t) \tag{2.18}$$

where $\mathbf{d}(v) = \langle v|\mathbf{r}|0\rangle$ is the atomic dipole matrix element for the bound-free transition state (but only the x component $d_x(v)$ will be used). The solution can be expressed in closed form, considering the vector potential $\mathbf{A}(t) = (A(t) = E\ cos(t), 0, 0)$, by the integral

$$\begin{aligned}b(v,t) = i\ &\int_0^t E\,dt''\,dt' cos(t') d_x(v + A(t) - A(t'))\times \\ &\times exp\left(-i\int_{t'}^{t}\left[(v + A(t) - A(t''))^2/2 + I_P\right]\right).\end{aligned} \tag{2.19}$$

[1]Note that the Volkov phase is related with the action by $S_v(t,t') = 2\Phi_V(p,t,t')$.

This result allows to write the x component of the dipole moment as

$$x(t) \equiv \langle \Psi(t)|x|\Psi(t)\rangle = \int d_x^*(v)\ b(v,t)\, d^3v + c.c.. \tag{2.20}$$

Note that here only the complex conjugate of the atomic dipole and the continuum amplitudes are present: only when C-C transitions are neglected $x(t)$ takes this form. Introducing the canonical momentum $p = v + A(t)$ and the quasiclassical action

$$S(p,t,t') = \int_{t'}^{t} \left(\frac{[p - A(t'')]^2}{2} + I_P \right) dt'' \tag{2.21}$$

it is possible to recover the three step physical interpretation of the process. In fact, looking at

$$x(t) = i \int_0^t dt' \int d^3p \underbrace{E\ cos(t') d_x(p - A(t'))}_{ionization} \underbrace{exp[-iS(p,t,t')]}_{propagation} \underbrace{d_x^*(p - A(t))}_{recoil} + c.c., \tag{2.22}$$

is possible to make this sequence:

1. $E\ cos(t') d_x(p - A(t'))$ represents the probability for the electron to tunnel and pass to the continuum at time t' with canonical momentum p;

2. the electron wave is then propagated freely moving in the laser field and acquiring, until the time t, a phase factor equal to $exp[-iS(p,t,t')]$;

3. the last step is the recombination at time t described by the amplitude $d_x^*(p - A(t))$.

The formula (2.22) can be generalized to a laser field $\mathbf{E}(t)$ arbitrarly polarized and enveloped but the restriction to linearly polarized monochromatic field is prefered for the majority of the experiments.

At this stage, it is possible to recall the first aim of this section: to reproduce teoretically the experimental harmonic spectra with their principal

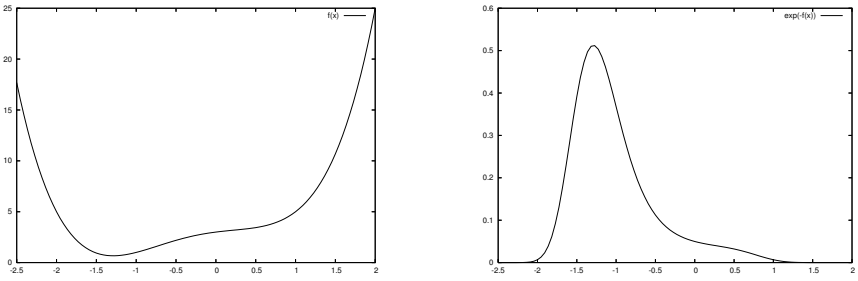


Figure 2.5: The basic idea of the saddle-point method is represented with these two figures: it is clear that a minimum for the function $f(x)$ is related to a maximum for the function $exp(f(x))$; so, integrating an exponential function, only the minima of the argument are contributing. So is possible to limit the calculation only on that extremal points called saddle-points.

highlights, i.e. the cut-off and the plateau . The presence of the exponential factor in the integral (2.22) suggest the method usually used in such situations, called saddle-point method. In fact, observing for example figure (2.5), is possible to note how the exponentital function modifies its argument: a minimum of the argument corresponds to a peak. So, since the extrmal points of the action $S(p,t,t')$ are for most contributing to the integral of $x(t)$, it is converted into a sum over these saddle-point. In order to identify these points, some considerations must be done on equation (2.22):

i) the dipole matrix elements that enter in (2.22) change typically on a scale of the order of $p^2 \simeq I_P$;

ii) $S(p,t,t')$ changes on a charateristic scale $p^2 \simeq 1/(t-t')$ (spreading due to quantum diffusion) and for $t-t'$ on the order of the laser period it varies much faster than any other term entering in (2.22).

Therefore the major contribution to the integral over p comes from the stationary points of the classical action satisfing:

$$\nabla_p S(p,t,t') = \mathbf{0}. \tag{2.23}$$

To conclude, the physical meaning of the last mathematical expression is clear by observing that

$$\nabla_p S(p,t,t') = \mathbf{x}(t) - \mathbf{x}(t').$$

The stationary points correspond to those momenta p for which the electron born at time t' returns to the same point at time t: the dominant contribution to harmonic emission is given by electrons which tunnel from the nucleus but recoil it while oscillating in the laser field. So the basic assumptions of the classical model -the three step model- can be deduced.
Applyng now the saddle-point method to (2.22), defining the return time $\tau = t - t'$ and the stationary x component of the momentum (the only one different form zero) $p_{st}(t,\tau) = E[cos(t) - cos(t-\tau)]/\tau$ (it allows the electron trajectory starting near the origin at time $t-\tau$, to return to the same position at t) the expression becomes

$$x(t) = i \int_0^\infty d\tau \left(\frac{\pi}{\varepsilon + i\tau/2}\right)^{3/2} d_x^*(p_{st}(t,\tau) - A_x(t)) \times \tag{2.24}$$
$$d_x(p_{st}(t,\tau) - A_x(t-\tau)) E\ cos(t-\tau) exp\,(-iS_{st}(t,\tau)) + c.c..$$

The factor $\left(\frac{\pi}{\varepsilon + i\tau/2}\right)^{3/2}$, where ε is an infinitesimal quantity, comes from the gaussian saddle-point integration. The quasiclassical action $S_{st}(t,\tau) = \int_{t-\tau}^{t} dt''(p_{st} - A(t''))^2/2$, in the limit $I_P \ll U_P$ tends to have the same stationary points τ_{st} as the classical one: like for the second assumption of the classical (semiclassical for Lewenstein) two-step model, this means that the electrons mostly contribuoting to the harmonics are not only those returning to the nucleus, but also those appearing with zero initial velocity $(v(t-\tau) = p_{st}(t,\tau) - A(t-\tau) = 0)$.
Now nothing is missing to complete some theoretical predictions: the spectrum is the Fourier transform of $x(t)$ and can be also resolved with saddle-point tecnique. From this last work what turns out is that the contributing phases are determined by the conservation law $(p_{st} - A(t''))^2/2 + I_P = 2m+1 = q$; physically, only the $(2m+1)$-th harmonics are emitted just when

they gain the right energy oscillating in the EM.
The last very important result coming from this analysis is the numerical evaluation of the absolute HHG cutoff law for $U_P \gg I_P$: the maxium harmonic order[2] is given by

$$N_{max} = 2K_{max} + 1 \simeq 3.17U_P. \tag{2.25}$$

To really appreciate this capital result is better to go back to the Fourier transform of the dipole matrix element. Since $S_{st}(t,\tau)$ is a linear function of $sin(2t)$ and $cos(2t)$ the (2K+1)-th Fourier component of x(t) can be calculated exactly:

$$x_{2K+1} = i\sum_{m=0}^{\infty}\int_0^{\infty} d\tau \left(\frac{\pi}{\varepsilon + i\tau/2}\right)^{3/2} \times e^{-iF_0(\tau)} b_{K-M} J_M(U_P C(\tau))(i)^M e^{iM\tau}, \tag{2.26}$$

where $C(\tau) = sin(\tau) - 4sin^2(\tau/2)/\tau$ and $F_0(\tau) = (U_P + I_P)\tau - 2U_P[1 - cos(\tau)]/\tau$. Since the Bessel function $J_K(U_P C(\tau))$ becomes exponentially small when $K > U_P C(\tau)$ than, for $U_P \gg I_P$, $N_{max} \simeq 2|C(\tau_{max})|U_P$. In fact, for $\tau_{max} \simeq 4.08$, the function has the first higher maximum at $2|C(\tau_{max})| \simeq 3.17$: it corresponds to the maximum of the kinetic-energy gain of the electron ionized at time t': in figure (2.6) is plotted $2|C(\tau)|$.

Another interesting aspect of this model is that many corrections, like the groud state depletion, can be considered to improve it. One important example is a surprising correction of the cutoff law: the well known formula $(2K+1)_{max} \simeq 3.17U_P + I_P$ (2.13), considering the absolute energy gain, is not correct if a saddle-point analysis is performed completely. To express the final result of this calculation the function $F(I_P/U_P)$ must be introduced:

$$(2K+1)_{max} \simeq 3.17U_P + F(I_P/U_P)I_P$$

The factor F is a slowly decreasing function starting at 1.32 where $U_P \gg I_P$ and approaching to 1. The quantum mechanical origin of this correction is

[2]It is interesting to note that in the range 2.4 $U_P < 2K < 3.17\ U_P$ only electrons returning into one laser cycle principally contribute to the HHG.

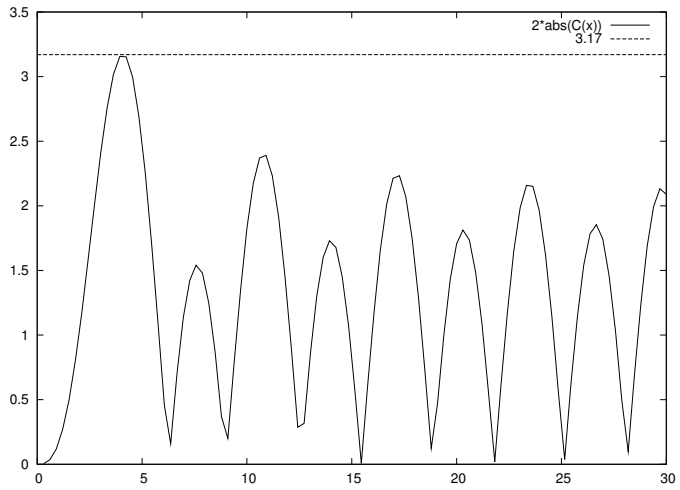


Figure 2.6: $2|C(\tau)|$ plot: the maxima correspond to the maximum achievable harmonic generation order.

that the electron tunneling and spreading were not included in the classical model: due to this effect the electron gains an energy, in its trajectory, higher than the amount predicted by the classical equation of motion.
To complete and improve the picture on this quasi-classical analysis now will follow a subsection discussing about the limits of this model and presenting an useful and equivalent description of this phenomena.

2.3.1 Fenomenological approach: quantum path

The model due to Lewenstein presented above is based on the hypotesis that when the electron is freed the Coulomb potential effects can be neglected: as a consequence of this assumption, as Brabec and Krausz underline in their work ([5],[9]), an underestimation of the ionization is made. So, considering only the ground state for the evolution of the system, the atomic dipole moment expectation value can be written as a sum of three probability amplitudes:

$$d(\tau) = \sum_{\tau_b} \frac{1}{\sqrt{i}}\ a_{ion}(\tau_b)\ a_{pr}(\tau_b, \tau)\ a_{rec}(\tau). \tag{2.27}$$

The sum is made on the retarded borning time $\tau_b = t_b - z/c$ when the electron tunnels into the continuum states; it involves:

1. ionization amplitude

$$a_{ion}(\tau_b) = \sqrt{\frac{dn(\tau_b)}{d\tau}}, \tag{2.28}$$

   where $n(\tau)$ is the free-electron density;

2. propagation amplitude

$$a_{pr}(\tau_b, \tau) = \left(\frac{c\pi}{\tau_b - \tau}\right)^{3/2} \frac{2I_P}{E(\tau_b)} exp(-iS), \tag{2.29}$$

   where

$$S = \int_{\tau_b}^{\tau} dt'[(p(\tau_b - \tau) - A(t'))^2 + I_P] \tag{2.30}$$

   and

$$p(\tau_b, \tau) = \frac{1}{\tau_b - \tau} \int_{\tau_b}^{\tau} dt' A(t'); \tag{2.31}$$

3. recoiling amplitude

$$a_{rec} = \frac{p(\tau_b - \tau) - A(\tau)}{(I_P + (p(\tau_b - \tau) - A(\tau))^2)^3}. \tag{2.32}$$

This formula clearly traces back to the three step model of Corkum and Kulander but with new general properties:

- the full electric laser field is used to calculate the single-atom dipole moment to account for nonadiabatic effects;

- Keldysh ionization rate is replaced by a static rate considering also the ground state depletion;

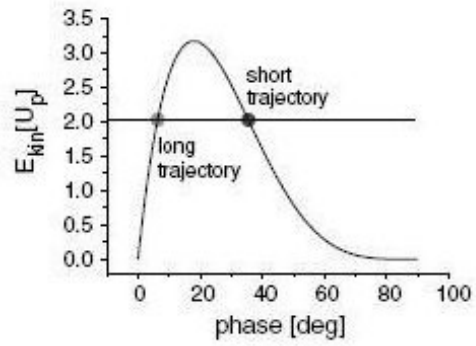


Figure 2.7: The two atomic phases leading to the same photon energy.

- writing the ionization amplitude as a function of the time-derivative of the free-electron density (2.28) the model is generalized to allow ground state depletion.

One important improvement of (2.27) is that it represents a sum over every possible quantum trajectory[3]. So the electrons, when passed in the continuum, have different trajectories and so different phases $\phi_{at} = S(p, t, t')$, called the atomic dipole phases. There are two principal trajectories and phases, corresponding to the same photon energy, contributing for most to the harmonic plateau; they are called longh and short trajectories since they differ in the time they spend in the continuum (figure 2.7). Depending on the respective ϕ_{at} they can interfere constructively or destructively. What is interesting for experimental application is that the electric field can modify the dipole phases and so is possible to control interference and, as a consequence, the harmonic generation process [8].

Before leaving this "microscopic" analysis ([9]) of the single-atom processes, and start studing the macroscopic effects due to the propagation, a note on the validity limits of this model is needed. The request that no bound state except for the ground state to partecipate to the HHG process is compatible with the strong field regime when $\gamma_K < 1$. So any contribution from other

[3]For numerical simulation this is the best way to describe the process.

kind of ionization is neglected. But this consideration is not always proper: in section (2.4) a more general approach will be discussed and described.

2.3.2 Propagation effects

From the "microscopic" analysis presented before, where single atom theory is described, many HHG features could be appreciated, but to have a complete picture of the physical phenomena also "macroscopic" effects must be considered. A theory, describing the propagation effects, must undertake every factor limiting the maximum achievable harmonic yield due to many body interactions like:

- dephasing;
- defocusing;
- absorption.

Propagation effects

The propagation of the high energy harmonics is influenced by the gas density, the presence of freed electron and by the geometry. For HHG there exist a certain interaction length, called coherence length, for which the harmonic efficency is higher: usually it goes from $1mm$ to $0.1mm$ [15][8]. The harmonic intensity can increase with the second power of the coherence lenght when the "phase-matching" condition is satisfied:

$$\Delta K = mk(\omega) - k(m\omega).$$

In this formula is considered only a collinear harmonic generation geometry: the harmonic propagated with the laser field; this approximation allow tho write the wavevector mismatch formula in scalar form.
The physical effects influencing ΔK are:

1. Δk_{disp} due to medium dispersion - usually gas - because of the dependence of the refractive index on ω;

2. Δk_{plasma}: to perform HHG high energy are needed and lots of electrons are freed; a plasma is generated giving resonances and dispersion;

3. Δk_{geom} is the contribution due to focalization and propagation of the wavevector.

Calculating each contribution the total mismatch,since $\Delta K_{vacuum} = 0$, can be found:

$$\Delta K = \Delta k_{plasma} + \Delta k_{dispersion} + \Delta k_{geom}.$$

What is important now is to determine how every single term acts; respecting the order of the previous item:

1. $\Delta k_{disp} = (n(\omega) - n(m\omega))\frac{m\omega}{c}$: since the refractive index is larger than 1 in the visible or near-infrared (nIR) and smaller than one in the XUV[4]; then $\Delta k_{disp} > 0$.

2. $\Delta k_{plasma} = \frac{\omega^2(1-m^2)}{2m\omega}$ so $\Delta k_{plasma} < 0$.

3. $\Delta k_{geom} = \Delta k_{foc} = \frac{2(m-1)}{b} > 0$: this means that the geometric effects are only due to the focusing of the EM and can be described just using the confocal parameter $b = 2z_R = \frac{\pi w_0^2}{\lambda}$ where w_0 is the waist size of the beam radius (see [8]).

In order to maximize the intensity of a certain harminic all these effects must be taken into account. The parameters on which was possilbe to act were: the position of the interaction zone with respect to the focus; the gas pressure and the noble gas (Ar, Ne, He, Xe).

Absorption

This limiting factor must be considered because photons in the soft x-ray energy range are typically absorbed by matter: having matter bound states in the 10-100 eV energy region the corresponding photoionization cross-section

[4]These characterisctic are choosen just to cover the majority of the experiments made on HHG

σ is high. So the absorption length $L_a = \sigma\rho$ increases with σ and also with the particle density ρ. To calculate the yield of the m-th harmonic an integral on the lenght L over the driving pulse must take into accout the continuous HHG inside matter and the immediate absorption:

$$I_m \propto \left| \int_0^L dz \rho A_m(z) exp\left(-\frac{L-z}{2L_a}\right) exp(i\phi_m(z)) \right|^2 . \tag{2.33}$$

In order to calcultate this value the harmonic amplitude of the single atom response $A_m(z)$ and the phase $\phi_m(z)$ must be known.

2.4 Different ionization processes

After the Lewenstein model was introduced for many years the principal task had been to extend his limitation over the tunneling limit. The relevant facts were that for such regime - where $\gamma_K \ll 1$ - the rate equation was computationally convenient and had good accuracy up to $\gamma_K \simeq 0.5$. At the same time, "preventing" more general studies, no simple closed-form could be found for the regime $\gamma_K \simeq 1$.

The principal hypotesis on which is based the described model is that the distortion due to the laser field is "slow" with respect to the evolution of the electron density: but is this quasi-static approximation always correct? No, increasing γ_K the electron ionization can happen through different processes like above-threashold or multi-photon ionization. But is possible to describe HHG as a function of the Keldysh parameter without limiting it only to the tunneling ionization?

Only in 2001 a general model was proposed by Yudin and Ivanov ([6]). They noted also that the existing studies (analytical expressions or numerical simulations) were not able not to obfuscate the subcyle dynamics of the electron while appearing in the continuum: there were multidimensional integral hiding this processes and any peculiar aspect (like the instantaneus phase dependence of the ionization during the "nonadiabatic tunnel ionization" as they call the other non-tunneling ionization processes). Throught their ana-

lysis they could distinguish, for arbitrary γ_K, the contribution to the total ionization probability between tunneling and multiphoton ionization: it was found that also for $\gamma_K \simeq 1$ the tunneling ionization preveals on the other regimes but it is significantly reduced with respect to the ideal condition required by Lewenstein. To understand how it is possible to parametrize ionization with γ_K the Yudin-Ivanov model must be described in detail.

For first, as for the Lewenstein model, the amplitudes of the quantum states involved in HHG processes are accurately defined. If the probability amplitude for the field-free continuum state $|v\rangle$ is $a_v(t)$ then the population of the continuum states is

$$W(t) = \int d^3v |a_v(t)|^2. \tag{2.34}$$

The single amplitude can be written with exponential accuracy - Dykhne method - as

$$a_v(t) \approx \int_{-\infty}^{t} dt' exp(-iS_v(t,t')). \tag{2.35}$$

Assuming that the envelope is nearly constant ($f \simeq 1$) during a laser pulse is possible to calculate the integral for $a_v(t)$ by saddle-point method: since t is the recoiling time the saddle-points most contributing to the integral are those ionization times t'_n such that $t'_n < t$. This points can be pulled in sequence starting from the nearest to t, t'_0; every t'_n satisfys

$$\begin{cases} [v_\parallel + sin(\Phi(t)) - sin(\Phi(t')) + \gamma_K^2] = 0 \\ Im[S_v(t,t'_n)] = Im[S_v(t,t'_0)], \end{cases} \tag{2.36}$$

where $\Phi(t) = \omega t + \phi_0$ and $v_\parallel$ is the electron velocity parallel to the electric field $\mathbf{E}(t) = \mathbf{E}_0 f(t) cos(\Phi(t))$.
The integral is replaced by a sum where every term, made on each saddle-point, represents a physical contribution to the continuum popolation $a_v(t)$:

- the population just appeared in the continuum at t is given by the integral on t'_0;

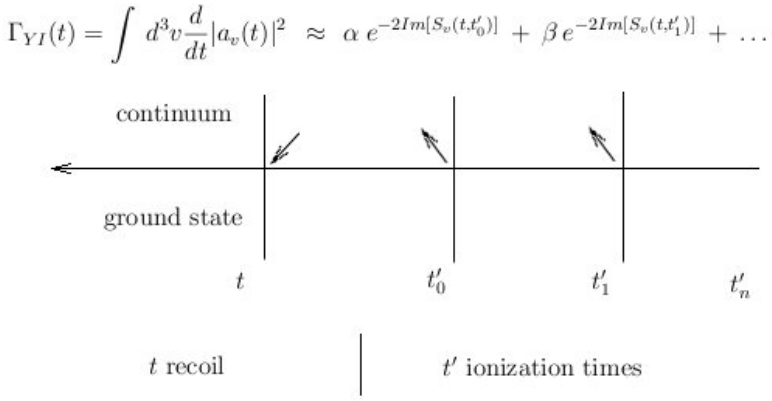


Figure 2.8: Representation of the saddle-point method used to reduce the integral of $\Gamma_{YI}(t)$ to a sum on few saddle-points. α and β are coefficients resulting form the gaussian intrgral on the ionization times t'_n.

- the contribution of $t'_n = t'_0 - 2\pi n$ for $n \geq 1$ describes the population created in the continuum one or more laser cycles ago (before t);

- only the t'_0-contribution must be taken into account when ionization at t is studied;

- since $v_\parallel^2/2 \ll I_P$ the exponent can be expanded with saddle-point method around $v_\parallel = 0$: so the predominant contribution is for non-moving electrons.

Introducing the phase $\theta(t) = \Phi(t) - \pi k$, so that $-\pi/2 \leq \theta(t) \leq \pi/2$, and $S_0(\theta(t)) = S_{v=0}(t, t'_0)$ than the istantaneous ionization rate becomes:

$$\Gamma_{YI}(t) = \frac{d}{dt}W(t) = \int d^3v \frac{d}{dt}|a_v(t)|^2 \approx \int d^3v e^{-2Im[S_v(t,t']} \approx e^{-2Im[S_0(\theta(t))]}. \tag{2.37}$$

So, solving the exponential factor, it can be written as:

$$\Gamma_{YI}(t) \simeq exp\left(-\frac{E^2 f^2(t)}{\omega^3}\Phi(\gamma(t),\theta(t)\right).$$

The Keldysh parmeter includes now the envelope by $\gamma = \frac{\gamma_K}{f(t)}$[5] and the expression for $\Phi(\gamma,\theta)$ is

$$\Phi(\gamma(t),\theta(t)) = (\gamma^2 + sin^2(\theta) + 1/2)ln(c) - \frac{3\sqrt{b-a}}{2\sqrt{2}}sin|\theta| - \frac{\sqrt{b+a}}{2\sqrt{2}}\gamma$$

where

$$a = 1 + \gamma^2 - sin^2(\theta),$$

$$b = \sqrt{a^2 + 4\gamma^2 sin^2(\theta)}$$

and

$$c = \sqrt{\left(\sqrt{\frac{b+a}{2}} + \gamma\right)^2 + \left(\sqrt{\frac{b-a}{2}} + sin|\theta|\right)^2}.$$

Several remarks must be done on these equations in order to confirm the obtained result :

i) for $\gamma \gg 1$ there is no θ dependence on Φ as in multiphoton regime;

ii) the phase dependence appears as γ decreases: is the effect of the tunneling ionization contribution;

iii) note that now the Keldysh ionization rate (2.7) can be obtained just setting $\gamma = 0$ (this request follows from i));

iv) the multiphoton regime can be reprocuced using $\Phi(\gamma, \pm\pi/2)$. Expressions composed by simple function of γ can be found for $\gamma \gg 1$ and for $\gamma \leq 2$.

At the end the rate can be expressed using a preexponential factor $N(t)$ as

[5]The envelope is treated as nearly constant during one-half of the laser cycle.

$$\Gamma_{YI}(t) = N(t) exp\left(-\frac{E^2 f(t)^2}{\omega^3}\Phi(\gamma(t),\theta(t))\right). \tag{2.38}$$

$N(t)$ can be deduced matching this rate with the averaged result rate (Perelomov, Popov, Terent'ev, Eksp '66 [14]); simplifying the result it can be written as

$$N(t) = C_{YI}(m,l)\left(\frac{3k}{\gamma^3}\right)^{3/2} I_P \left(\frac{2(2I_P)^{3/2}}{Ef(t)}\right)^{(2/\sqrt{2I_P})-|m|-l},$$

$$k = ln(\gamma + \sqrt{\gamma^2+1} - \frac{\gamma}{\sqrt{\gamma^2+1}}).$$

It is intresting to compare this result with the Ammosov-Delone-Krainov static rate (the $C(m,l)$ factors depend on the angular momentum l and on the magnetic quantum number m)

$$\Gamma_{ADK} = C_{ADK}(m,l)\sqrt{\frac{E}{(2I_P)^{3/2}}} I_P \left(\frac{2(2I_P)^{3/2}}{E}\right)^{(2/\sqrt{2I_P})-|m|-l} \times$$

$$\times exp\left(-\frac{2(2I_P)^{3/2}}{3E}\right). \tag{2.39}$$

The principal difference is the presence of $\gamma(t)$ in $\Gamma_{YI}(t)$: in Γ_{ADK} the pulse envelope $f(t)$ is considered to be constant while to calculate Γ_{YI} is asked not to change during an half-cycle time. Since the pulse shape and duration is very important for strong-field phenomena as HHG it is clear haw this result is important to analyze the process.

The general rate obtained in this section allow to change the ionization regime, changing γ_K, depending on the particular experiment; in order to study the different contribution to the harmonic generation (see chapter 4) it represent an interesting instrument to parametrize the ionization process as a function of $\gamma(t)$. The exponential factor of $\Gamma_{YI}(t)$ also shows that, for non-tunneling regimes, the subcycle dynamics plays a key role in the first step of the HHG: it determines, for exemple, the direction of the final drift velocity of the freed electrons in a typical experimental regime of $\gamma \simeq 1$ and, as a consequence, the harmonic yield.

Chapter 3

Experimental set-up

The experimental set-up for HHG experiment is described in this chapter. In order to characterize the phenomenon different configuration were choosen with respect to the objectives of the measurements. In particular in every experiment two frequencies are used for harmonic generation: as seen in chapter 2, the ionization regime depends on the EM field source and so, changing the EM radiation, the process can be analyzed accurately. In fact, even the laser EM source, described in section (3.1), and its second harmonic will be used for the harmonic generation in order to compare the tunneling regime for $\gamma_K \ll 1$, with the IR, and an intermediate for $\gamma_K \simeq 1$ (see [13]). The optical apparatus for the generation and acquisition system will be described in section (3.3).

3.1 Laser system

In the previus chapter the importance of the EM field was deeply underlined: to study HHG phenomena some minimal pulse properties are required. For this reason the described commercial Laser system was chosen to perform this kind of experiment.

The Laser system is composed by a Ti:Sa oscillator and a regenerative amplifier. The oscillator is pumped by a Neodymium Vanadate (Nd:YVO4)

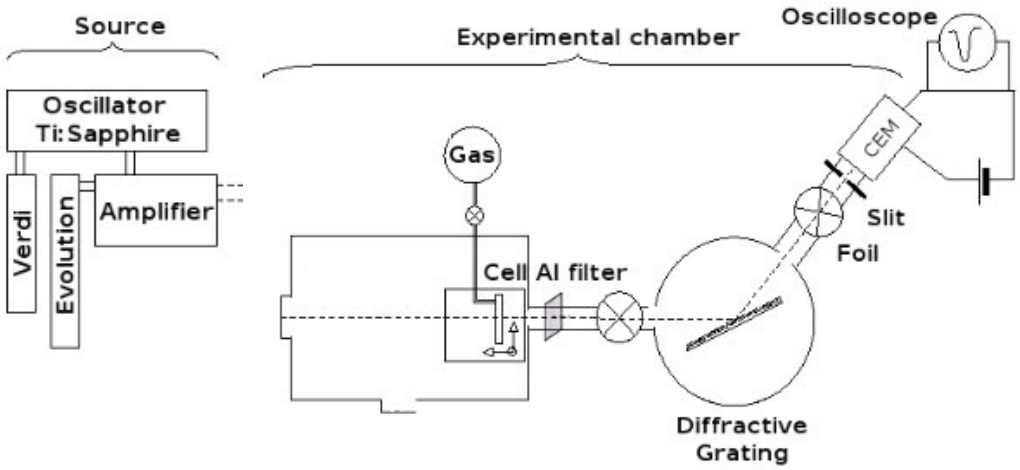


Figure 3.1: Laser components (left): Verdi, Ti:Sa Oscillator, Evolution and Amplifier. Experimental chambers (right): generation chamber and acquisition chamber.

continuum laser at $532nm$ and $5W$. The mode-locking of the modes allows the generation of femtosecond pulses with a band-width between 45 and 55 nm. These pulses are sent to a grating stretcher and amplified. The central wavelength is usually set to $796nm$ ($\approx 1,5eV$, near IR) in the oscillator cavity. Before entering into the regenerative cavity of the amplifier, the pulses are stretched to some tens of picoseconds, in order to avoid damages to the amplifier's crystal. The permanence time of the light pulses inside the cavity is controlled by two Pokel-cells in order to have the optimum number of round-trips inside the amplifier. Pulses are then compressed to $\simeq 50-60fs$. The delivered light pulses have the central wavelength at $796nm$, $1kHz$ repetition rate, horizontal polarization, time width of $\simeq 60fs$ and average output power after the amplification of $\simeq 2.2W$.

3.2 Experimental chambers

The experimental chamber is divided into two parts:

- the HHG chamber: the beam is focused on a static cell where it inter-

acts with a noble gas at $10^{-3}mbar$;

- the monocromator chamber: it is composed by a rotating grating and a slit in order to select a single wavelength of the EUV radiation generated in the first chamber; than a photo-multiplier, a Channeltron (Channel Electric Multiplier), allows to measure the electric signal generated by photo-elettric effect and related to the number of photons of the radiation.

Observe that the chambers can be isolated to prevent damage to the CEM and that the generated EUV ($15 - 80nm$) radiation, collinear with the laser beam, is filtered by a thick alluminium sheet ($200nm$) in order to reduce the intense IR radiation.
Inside the first chamber the beam is focused by a convex mirror or two lenses. The HHG alluminium cilindric cell, $10mm$ of diameter and length 3 or $7mm$, is closed with a alluminium sheet: both IR and second harmonic can make the hole and interact with the inner noble gas at working pressure $\approx 10^{-3}mbar$. Then the monocromator is composed by a diffractive grating (grating density $576mm^{-1}$) and a slit. It is optimized to reflect at EUV energies: it has a spherical profile (radius of $1m$) and allow a resolution of 0,1-45 nm. The angular position is controlled by a step-by-step engine: a software controls the position and the CEM signal is measured and saved thanks to a digital oscilloscope and a Labview acquisition program. The CEM voltage is set to a value from 1000V to 1900V depending on the experimental conditions.

3.3 HHG facility

As underlined in section (2.4) the Keldysh parameter γ_K parametrizes the ionization process. In order to perform measurements at different ionization regimes two set-up were built: one to generate separately with IR and its second harmonic and one to study the process as a function of γ_K.

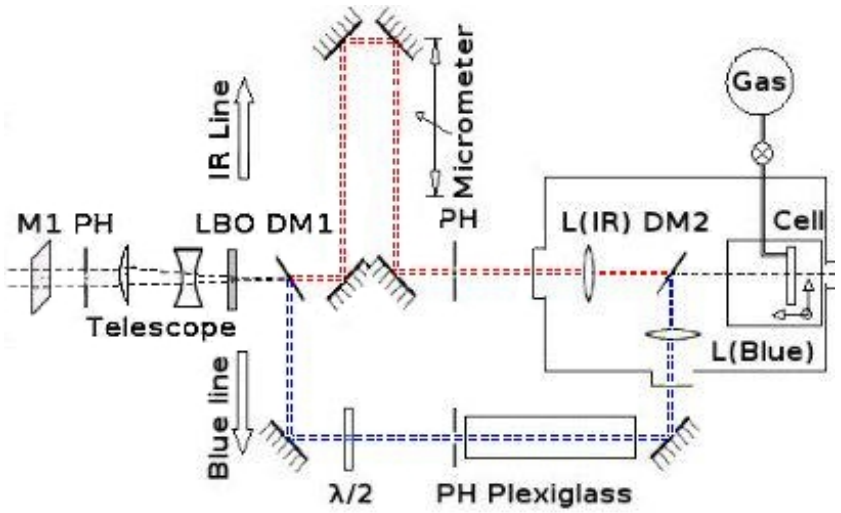


Figure 3.2: Optical set-up to generate separately with IR and its second harmonic, Note that two lenses are used in order to control chromatic aberration. In the figure: PH are the pin-holes, M high reflectivity silver mirrors, $\lambda/2$ the retarded plate, L are the lenses and DM are the dichroic mirrors

Both set-up will be described in next subsections. Note that, in order to measure with both IR and second harmonic at the same experimental condition (phase-matching, radiation characteristic, gas pressure and focus position) the set-up are versatile and allow to change immediatly configuration. The systems can be considered useful sources of EUV radiation $(15 - 80nm)$ at $1kHz$ R. R. as will be oberved in chapter 4.

3.3.1 Two-color optical set-up

The beam generated by the amplifyer, horizontally polarized, is reflected by four high reflectivity mirrors (in figure (3.2) identified by M) and two pin-holes are used to simplify the daily adjustment. With a telescope, composed by a plane-convex lens and a bi-concave lens, the laser spot is reduced in order to optimize the transmission through a LBO (Litium Triborate LiB_3O_5)

non-linear crystal (1,5mm): as a consequence of the interaction with the medium the second harmonic of the fundamental frequency is generated with an efficiency of $\approx 25\%$ and ortogonal polarization with respect to the IR radiation.
The two collinear beams then are split by a dichroic mirror optimized to reflect at 45° the radiation at $400nm$; so the second harmonic, completely reflected, passes through a $\lambda/2$ sheet in order to control and modify the beam polarization.
The two branches are separately focused with two optimized lenses ($200mm$ for IR and $170mm$ for second harmonic) and then recombined with a dichroic mirror. On the IR-branch a micrometer is installed; it allows to change the optical length in order to have the temporal coincidence with the second branch. The cell, described in section (3.2), is positioned exactly on the focus position. Note that its position can be regulated also during the measurements in order to modify the phase-matching conditions related to the focus position.

The set-up is used to measure spectra with IR and $400nm$ at their maximum power. It is possible for example to change the intensity of the second harmonic rotating the LBO crystal but the pulse length was not preserved. In order to limit the variation to only the incident number of photons another arrangement is set.

3.3.2 Intensity variation optical set-up

The substantial difference with the set-up described above is that the IR beam, after the telescope, is split with an intensity variable ultra-fast beam-splitter composed by a $\lambda/2$ retarded plate and two Brewster mirrors. It allows to regulate the intensity of the two beams without changing the polarization of them:

- the transmitted beam (form the first window) is horizontally polarized is used to generate the second harmonic with a BBO ($beta - BaB_2O_4$,

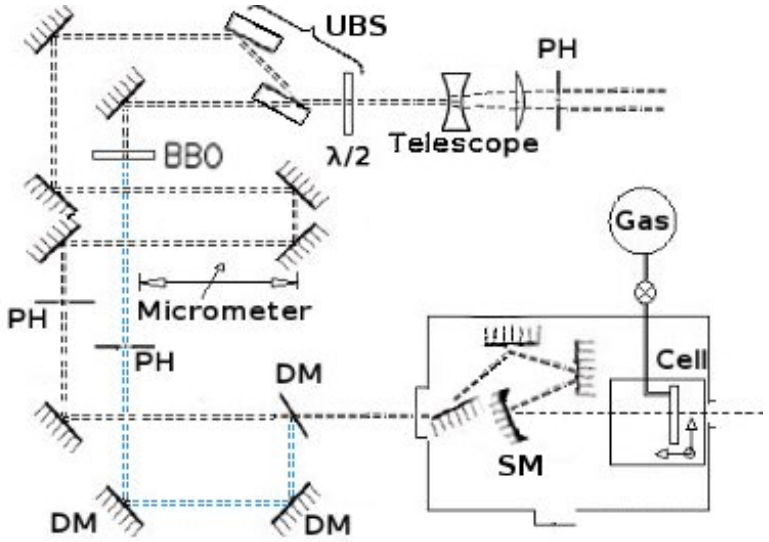


Figure 3.3: Second optical set-up; it allow to study HHG as a function of the Keldysh parameter γ_K. Legend: BBO is the second harmonic crystal, DM are the dichroic mirrors, UBS is the ultra-fast beam splitter, PH are the pin-holes, SM is the spherical mirror and the other represented mirrors are silver coated type.

it has an higher efficiency, $\approx 33\%$) crystal;

- the second IR beam is reflected by the two Brewster mirrors and has vertical polarization.

On the IR branch a micrometer is installed in order to change its optical length. Then the beam is reflected with a silver mirror in the experimental chamber direction. It intercepts the last dichroic mirror of the second harmonic branch and the two beams recombines. Note that second harmonic, before beeing recombined, is reflected by three dichroic mirrors in order to eliminate the IR radiation still collinearly propagating with it.
The collinear beams then enter inside the first experimental chamber. They are reflected by three silver mirrors and then are focused on the cell by a spherical silver mirror. This configuration is chosen in order to perform measurements with both IR and its second harmonic. The property of this

set-up is that the intensity can be changed: is possible to study the HHG as a function of the Keldysh parameter γ_K without modifying the pulse envelope. In particular a spherical mirror is used for this experiment since it does not suffer of chromatic aberration; the characteristics of the ultra-fast beam-splitter is that it does not modify the focus position as instead filters do: so, once the spatial coincidence is obtained, it is preserved for the whole experiment. The combination of this two devices assures the spatial and the temporal coincidence of focus with respect to the position of the cell even changing the radiation intensity of the beams.
For two color measurements the temporal coincidence was obtained generating the third harmonic as $1\omega + 2\omega$ with a LBO crystal.

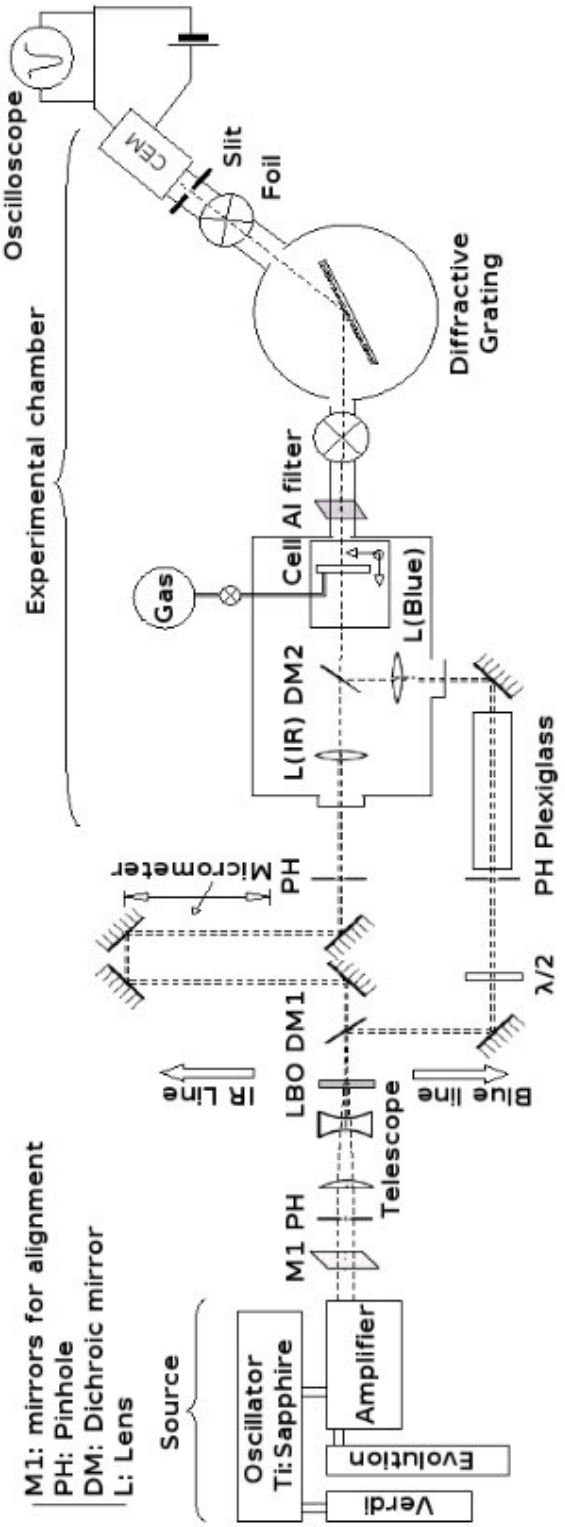


Figure 3.4: Complete experimental set-up for the generation at $800nm$ and $400nm$.

Chapter 4

Measurements and analysis

In this chapter two measurements will be described:

- the HHG with IR and its second harmonic: the process will be characterized showing that the set-up can be used as a EUV source;
- characterization of the HHG variating the Keldysh parameter.

The principal aspect of both experiment is that the ionization regime changes from tunneling, when generating with IR, to at least an intermediate regime, when the second harmonic is used. This difference make possible to compare the measurements even if the IR intensity is four times the second harmonic intensity; in fact the efficiency of the generation with radiation at $400nm$ wavelength is considerably higher.
In section (4.1) single measurements with IR and second harmonic, using Ar and Ne, will be described; the result are compared in order to evaluate the HHG efficiency for both frequencies. In section (4.2) are presented the measurements of the ionization dependence form the Keldysh parameter.

4.1 IR and second harmonic HHG

The experimental set-up for these measurements is described in section (3.3.1). The radiation used for the HHG is:

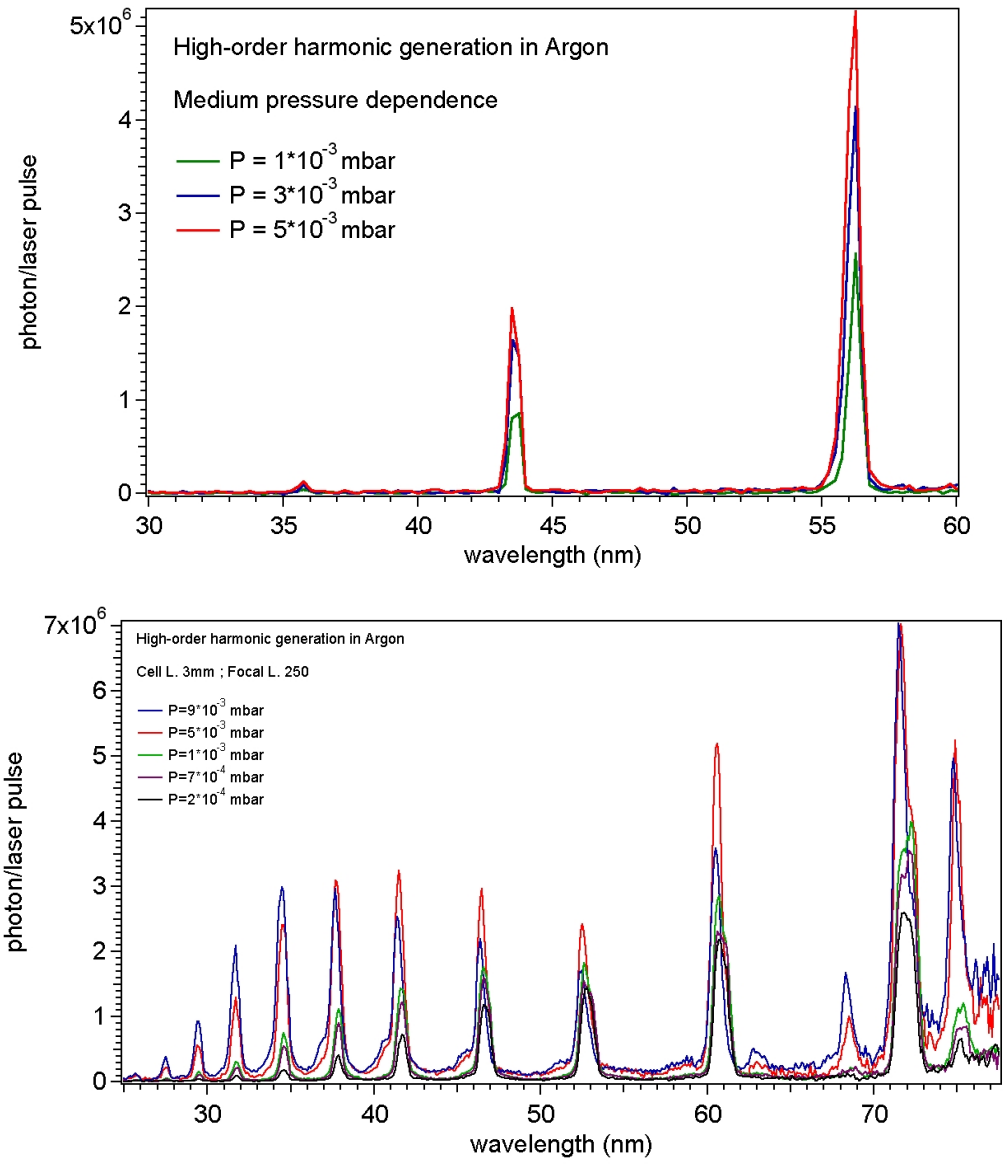


Figure 4.1: HHG in Ar using second harmonic (top) and (bottom) IR radiation.

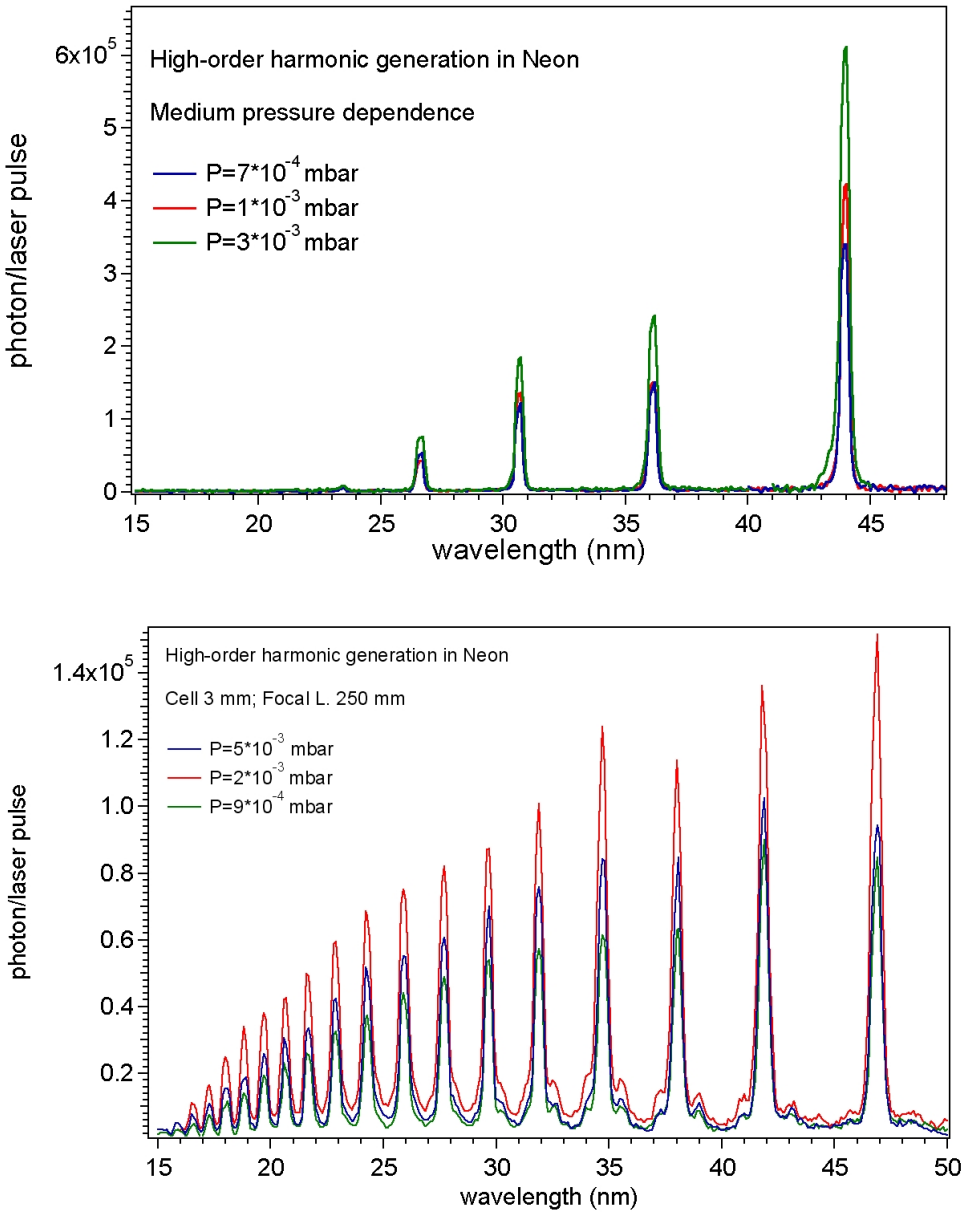


Figure 4.2: HHG in Ne using second harmonic (top) and (bottom) IR radiation.

- IR at $796nm$, $2.2mJ$ per pulse, temporal length $\simeq 50fs$;
- Second harmonic at $398nm$, $380 - 480\mu J$ per pulse, temporal length $\simeq 75fs$.

In order to optimize the set-up before every experiment the second harmoni efficiency is measured end increased regulating its angle and the spot size with the telescope. When the vacuum is made on the first chamber the hole is made with both frequancies. Before starting the acquisition the gas pressure and the CEM voltage are preliminarly analyzed: usually the ampitude of a single harmonic is directly observed in the osciloscope in order to set the best phase-matching pressure conditions. In fact the generation efficiency strongy depends on this parameter.
In order to evaluate the pressure dependence some measurements are performed with Ar and Ne form $\simeq 2\ 10^{-4}mbar$ to $\simeq 9\ 10^{-3}mbar$ using both frequencies. The data show the typical HHG behavioyr as described in chapter 2: non-perturbative region, plateau region of constant efficiency and than the cut-off. Observe that, since the radiation is different, the harmonic spacing is not the same.

In figures (4.1) HHG in Ar is reported. Is possible to observe the phase-matching conditions due to the pressure variation: the response of each harmonic is different. Generation in Ne with the same conditions is on figures (4.3).
Observing the spectra is possible to underline the principal difference of the HHG with IR and the second harmonic. The number of harmonics of the IR generation is higher: it simply follows from the fact that only odd harmonics of the laser frequency are produced; since the peak position scales as $\lambda/(2m+1)$ is obvious that every two IR-harmonics only one from the second harmonic is present. Since the energy of the second harmonic is lower the cut-off is shifted at higher wavelength; this aspects, clear in the reported spectra, also explains why the HHG classical behaviour (chapter 2) is harder

Figure 4.3: In this figure are represented the spectra obtained in Ne and Ar, at the best phase-matching condition, in order to compare the process between IR and second harmonic generation.

to observe in the $400nm$ generation. In fact, looking at the spectra generated in Ar, it seems that no plateau is present. It does not mean that there is no HHG since instead in Ne is possible to recognize the plateau between the cut-off and the non-perturbative region.
It is interesting to compare the higher generated harmonics. In the HHG with the second harmonic the maximum photon rate is at $44nm$ in Ne (9^{th} harmonic) and at $57nm$ in Ar (7^{th} harmonic) respectively producing $\simeq 6 \times 10^8 ph./s$ and $\simeq 5 \times 10^8 ph./s$ at $\simeq 1 \times 10^{-3} mbar$. The photons with higher energy correspond to the 19° harmonic in Ne ($\simeq 21nm$ or $60eV$) and to the 11° in Ar ($\simeq 36nm$ or $35eV$).
Note that it is possible to identify absorption effects. Each harmonic in fact increases while increasing the pressure inside the cell but at 5×10^{-3} it starts decreasing: this is due to gas reabsorption.

Since the objective of this measurements was to compare the ionizations regime in figure () and () are drawn the spectra obtained with IR and $400nm$ in Ne and Ar respectively. In order to estabilish the principal difference the plateau range and the cut-off position will be taken into account. The HHG with IR in Ne, with respect the the Ar, moves the plateau region from $\approx 40 - 55nm$ to $\approx 25 - 45nm$. Instead with $400nm$ the plateau is present only in Ne from$\approx 25nm$ to $\approx 35nm$. Since the pondermotive potential U_P is higher for the IR radiation also the cut-off corresponds to higher photon energies.
But the interesting aspect to underline is that the photon number per pulse is comparable even if the energy per pulse of the $400nm$ radiation is four time lower with respect to the IR. This translates into an higher generation efficiency. In fact, considering two harmonics in Ne inside the plateau region,

the efficiency for $400nm$ is $\approx 10^{-10}$ while for the IR is $\approx 10^{-11}$; in Ar the efficiency is 10^{-9} for $400nm$ and 10^{-10} for IR. This phenomenologial effect is explained by Lewenstein in [7]. In fact, for higher laser frequency, the electronic wave function spreading, reducing the recoiling probability, is lower; the fact that the number of harmonics is lower also increases the conversion efficiency for the last orders since the number of ionized photons is shared by less harmonics.

4.2 Ionization as a function of γ_K

In order to study the HHG variating the Keldysh parameter the optical set-up was modified adding the ultra-fast beam splitter. It allow, rotating the angle of the retarded plate, to change the power of the branches without influencing the focus position or the pulse length.
The preliminar operation are the same described in the previous section: allinement, temporal and spatial coincidence, optimization and evauation of the phase-matching conditions (pressure and focus position). The principal difference is that the ampitude of the higher harmonics was measured reducing the power per pulse. The CEM voltage was every time increased in order to have a cear signal on the oscilloscope.
In figures () and () the HHG with the second harmonic in Ne is reported respectively for the 7-th and 9-th harmonic. The number of photon per pulse is potted as a function of γ_K. In figure () the same graph is potted generating in Ar. The error on the y-axes is simply the harmonic FWHM. Is clear that the harmonic ampitude decreases with $gamma_K$; this follow from the fact that the Kesldysh parameter was increased by reducing the pondermotive potential, i.e. reducing the power of the incident radiation.
Observe that the limit of the generation is related to the acquisition system. Depending on the analyzed harmonic different values of $gamma_K$ were reached; but it is interesting to study the harmonic amplitude dumping. In fact, as underined in section (2.4), the keldysh parameter parametrizes the

Figure 4.4: Number os photons per pulse For a single harmonic: $44nm$, $56nm$ in Ar and Ne.

ionization processes: this means that the HHG pass from the tunneling regime (or an intermediate one) to the multi-photon regime.

4.3 two and three color generation

4.4 Data analysis

4.4.1 Two color single HHG

4.4.2 γ_K parametrization

Chapter 5

Conclusions

Conclusioni

Appendix A

Lewenstein model

the ground state $|0\rangle$ with amplitude $a(t) \simeq 1$, and on the continuum states $|v\rangle$[1] ($b(v,t)$ are their amplitudes) as

This equation expresses the probability distribution on the allowed quantum states of the HHG process; selecting the continuum states the bound-free transition can be considered as a "simple" scalar product of wave function superposition. That is why is so important to choose the continuum set of states.

The integral action S_v is defined using the orthogonal velocity components $v_\parallel$ and $v_\perp$ - respectively parallel and perpendicular to the amplitude E - and the electron velocity amplitude oscillation in the laser field $v_0 = E/\omega$ (ω is the laser frequency; $f(t)$ the pulse envelope so that the amplitude is $E\ f(t)cos(\omega t + \phi_0)$):

$$S_v(t,t') = (I_P + \frac{1}{2}v_\perp)(t-t') + \frac{1}{2}\int_{t'}^{t} dt''[v_\parallel + v_0 f(t)sin(\Phi(t)) - v_0 f(t'')sin(\Phi(t''))]^2 \tag{A.1}$$

[1]These are the quantum solution for an electron feeling an EM, they are konwn as Volkov states; in section 2.4 a more detailed description will be given.

Bibliography

[1] P. Corkum, N. H. Burnett, and F. Brunel, *Phys. Rev. Lett.*, **62**, 1259 - 1262 (1989).

[2] P. Corkum, *Phys. Rev. Lett.*, **71**, 1994 (1993).

[3] K. C. Kulander,J. K. Schafer, and J. L. Krause *Proc.Work-shop on Super-intense Laser Atom physics(SILAP)*, (1993).

[4] K. C. Kulander,J. K. Schafer, and J. L. Krause *Phys. Rev Lett.*, **68**, 3535 (1992).

[5] M. Geissler, G.Tampea, and T. Brabec, *Phy. Rev. Lett.*, **62**, 033817 (2000).

[6] G. Yudin, M. Ivanov, *Phy. Rev. Lett.* **49**, 013409 (2001).

[7] M. Lewenstein, Ph. Balcou, Y. Ivanov, A. L'Huillier, and P. Corkum, *Phy. Rev. Lett.*, **49**, 3 (1994).

[8] T. Pfeifer, C. Spielman, and G. Gerber, Femtosecond x-ray science, *Rep. Prog. Phys.*, **69**, 443 - 505 (2006).

[9] T. Brabec, F. Krausz, Intense few-cycle laser fields: Frontiers of nonlinear optics, *Rev. Mod. Phys.*, Vol **72**, No. 2 (2000).

[10] L. V. Keldysh, *Sov. Phys.*, –JEPT, **20**, 1307 (1965).

[11] M. V.Ammosov, N. B. Delone, and V. P. Krainov, *Sov. Phys.*, –JEPT, **64**, 1191 (1986).

[12] G. G. Paulus, W. Nicklich, Huale Xu, P. Lambropoulos, and H. Walther, *Phys. Rev. Lett.* 72, 2851 - 2854 (1994).

[13] C. Lynga, A. L'Huillier, and C-G. Wahlstrom *J. Phys. B: At. Mol. Opc. Phys.* **29**3293-3302 (1996).

[14] A. M. Perelomov, V.S. Popov, and M.V. Terent'ev, Zh. Eksp, *Teor. Fiz.* **50**, 1393 (1966)[*Sov. JEPT* **24**, 207(1967)].

[15] E. Gibson et al, *IEEE Journal of selected topics in quantum electronics* **10**, no. 6 (2004).

Ringraziamenti

...